Sirt3 deficiency impairs AMPK–Acc1 antilipogenic signaling in female adipocytes

Ena Šimunić[1#], Kate Šešelja[1#], Iva I Podgorski[1], Robert Belužić[1], Marijana Popović Hadžija[1], Marija Pinterić Mavar[1], Mirta Rešetar[1], Mirna Halasz[1], Morana Jaganjac[1], Ivana Tartaro Bujak[2], Marta Protrka[3], Tihomir Balog[1], Sara Stojanović[4], Aleksandra Korać[4], Sandra Sobočanec[1]*

[1]*Division of Molecular Medicine, Rudjer Boskovic Institute, Zagreb, Croatia*

[2]*Division of Materials Chemistry, Rudjer Boskovic Institute, Zagreb, Croatia*

[3]*University of Zagreb Faculty of Science, Department of Biology, Zagreb, Croatia*

[4]*Faculty of Biology, Center for Electron Microscopy, University of Belgrade, Belgrade, Serbia*

[#]*equally contributed*

**corresponding author; ssoboc@irb.hr*

Abstract

Background: Biological sex influences adipose tissue function, while impaired adipogenesis contributes to adipose dysfunction. Sirtuin 3 (Sirt3), a mitochondrial NAD+-dependent deacetylase involved in oxidative metabolism and stress adaptation, remains insufficiently defined in adipogenic differentiation. We investigated how Sirt3 and sex shape adipogenic phenotype in mouse embryonic fibroblast (MEF)-derived adipocytes. **Methods and Results:** Male and female Sirt3 wild-type (WT) and knockout (KO) mouse MEFs were differentiated into adipocyte-like cells and analyzed by Oil Red O staining, confocal microscopy, lipid droplet morphometry, adipogenic gene expression, fatty acid profiling, LC–MS metabolomics, immunoblotting, and transmission electron microscopy (n = 3–5 biological replicates per group). All groups induced adipogenic marker expression and formed lipid rich adipocyte-like cells, with female KO adipocytes showing the strongest lipid storage phenotype. In females, bortezomib (BTZ) increased AMPK and Acc1 phosphorylation in WT adipocytes, whereas KO cells showed reduced basal pAMPK/AMPK and failed to mount a comparable AMPK–Acc1 response. AICAR failed to restore AMPK–Acc1 signaling in KO adipocytes. Sirt3 deficiency increased Scd1 abundance and the C16:1/C16:0 desaturation index. BTZ reduced Scd1 in KO cells without normalizing the elevated desaturation ratio. Metabolomics indicated predominantly BTZ-associated glycerophospholipid and lysophospholipid remodeling. Qualitative ultrastructural analysis revealed BTZ-associated organelle stress, most evident in KO adipocytes. **Conclusions:** Sirt3 deficiency promotes a female biased lipid storage phenotype linked to impaired AMPK–Acc1 antilipogenic signaling, reduced lipid turnover, and persistent Scd1-associated fatty acid desaturation, supporting a model in which female adipocytes rely on Sirt3-dependent metabolic control during adipogenesis.

Keywords: Sirtuin 3; sex differences; adipogenesis; *de novo* lipogenesis; AMPK–Acc1 signaling; bortezomib

Introduction

Adipose tissue metabolism exhibits pronounced sexual dimorphism, influencing susceptibility to obesity-associated metabolic dysfunction in experimental models [1]. Obesity-related phenotypes reflect not only excess energy storage but also dysregulation of tissue-specific metabolic pathways [2]. In mice, females often display a comparatively more favourable metabolic profile than males, driven in part by sex differences in adipose tissue distribution and function. Females preferentially accumulate subcutaneous adipose tissue, which is associated with improved insulin sensitivity and reduced cardiometabolic risk [3]. Hormonal regulation and mitochondrial function further contribute to sex-specific control of lipid metabolism and energy balance [4]. Adipose tissue is a central regulator of energy homeostasis, and its dysfunction under metabolic stress is closely linked to obesity-related pathologies. In addition to its role in energy storage, adipose tissue functions as an active endocrine organ, secreting adipokines and lipid-derived mediators that regulate systemic metabolic homeostasis. Chronic nutrient excess disrupts these functions, promoting inflammation, insulin resistance, and ectopic lipid deposition. Adipogenesis, the differentiation of preadipocytes into mature adipocytes, is essential for establishing adipose tissue function and cellular specialisation. Efficient adipogenesis supports adipose tissue expansion through hyperplasia, which is metabolically protective compared with adipocyte hypertrophy. Conversely, impaired adipogenesis contributes to adipose tissue dysfunction and the progression of metabolic disease [5]. Most current insights into adipogenic differentiation are derived from *in vitro* studies using murine preadipocyte cell lines, primarily

3T3-L1 and 3T3-F442A [6]. Although these models have been widely used to define central adipogenic pathways, they represent relatively homogeneous, lineage-committed systems. In contrast, the adipogenic potential of mouse embryonic fibroblasts (MEFs) has been explored to a lesser extent [7, 8]. MEFs provide an adaptable *in vitro* model for studying adipogenic differentiation under diverse genetic and environmental contexts, as they retain the capacity to undergo adipocyte differentiation in response to defined adipogenic stimuli [9].

Sirtuin 3 (Sirt3), a conserved NAD^+-dependent mitochondrial deacetylase, plays a central role in regulating mitochondrial metabolism by activating enzymes involved in fatty acid oxidation, oxidative phosphorylation, and antioxidant defence [10]. By modulating the acetylation status of key metabolic and redox proteins, Sirt3 maintains mitochondrial efficiency and limits oxidative stress under conditions of metabolic demand. Reduced Sirt3 expression has been linked to impaired insulin signalling and the development of diabetes and related metabolic disorders [11, 12]. These findings highlight Sirt3 as a critical regulator of metabolic flexibility and insulin sensitivity. In line with these observations, Sirt3 KO mice subjected to a high-fat diet show increased susceptibility to metabolic syndrome, including insulin resistance, dyslipidaemia, and hepatic steatosis [13]. Our previous studies demonstrated a male-specific reduction in Sirt3 expression in response to nutritive stress [14]. Moreover, female mice deprived of sex hormones showed increased vulnerability to high-fat diet-induced metabolic stress [15], underscoring the importance of sex-dependent regulatory mechanisms. Consistently, our *in vitro* data revealed a significant impact of Sirt3 on female-specific susceptibility to etoposide-induced DNA damage in MEFs, a key contributor to cellular ageing [16]. Although Sirt3 is a well-established regulator of metabolic homeostasis, its role in adipogenic differentiation remains poorly defined. Here, we demonstrate that adipogenic

differentiation efficiency in MEF-derived adipocytes is significantly modulated by Sirt3 and biological sex, revealing a previously unrecognised role for Sirt3 in the sex-specific regulation of adipogenesis and lipid metabolism.

Methods

Cell Culture

Mouse embryonic fibroblasts (MEFs) were isolated from embryos of both sexes derived from 129S1/SvImJ wild-type Sirt3$^{+/+}$ (WT) (Stock No: 002448, Jackson Laboratory, Bar Harbor, ME, USA) and Sirt3$^{-/-}$ (KO) (Stock No: 012755, Jackson Laboratory, Bar Harbor, ME, USA) mouse lines, following the protocol described in [17]. Each embryo was processed separately to enable sex-specific analyses. The cells were cultured in a controlled environment at 37°C with a carbon dioxide concentration of 5%. Sex determination of the MEF was conducted through PCR analysis, employing specific primers that target the sex-determining region Y (Sry) gene located on the Y chromosome, thereby enabling the differentiation between male and female MEF. MEF were then immortalized using a plasmid with the SV40 promoter and grown in an incubator at 37°C and 5% CO_2, in DMEM medium supplemented with 10% fetal bovine serum (FBS Advanced, Capricorn Scientific GmbH, Ebsdorfergrund, Germany; Cat. No. FBS-11A), 1% antibiotic/antimycotic mixture, 1% non-essential amino acid (NEAA) mixture, and 50 µM β-mercaptoethanol. The MEF utilized in this study consisted of biological replicates, with each replicate being derived from a single embryo per experimental group, resulting in four distinct groups generated from four individual embryos.

Differentiation of MEF into Adipocyte Lineage

MEF-derived adipocytes refer to heterogeneous cultures of mouse embryonic fibroblasts subjected to adipogenic differentiation, containing adipocytes at various stages of maturation along with residual non-adipogenic cells (for concision, adipocytes in the following). Their differentiation was obtained by the following protocol (Figure 1A): Sirt3 WT and Sirt3 KO MEF of both sexes were seeded at 5 × 10^5 cells per well in 6-well culture plates and 1.5 × 10^5

cells per well in 24-well culture plates. Cells are grown in an incubator at 37°C and 5% CO_2, in DMEM medium supplemented with 10% fetal bovine serum (FBS Advanced, collected in South America; Capricorn Scientific GmbH, Ebsdorfergrund, Germany; Cat. No. FBS-11A), 1% antibiotic/antimycotic mixture, 1% NEAA mixture, and 50 µM β-mercaptoethanol), as described above. One day post-confluency (Day 0), cells were induced into adipogenesis with differentiation medium according to [9]. Differentiation medium contained 0.5 mM 3-isobutyl-1-methylxanthine (IBMX) (Sigma Aldrich, I5879), 10 µg/mL insulin (Sigma Aldrich, I0516), 1 µM dexamethasone (Sigma Aldrich, D4902) and 5 µM rosiglitazone (Sigma Aldrich, R2408). After 3 days (Day 3), the medium was changed to medium containing 10 µg/mL insulin and 5 µM rosiglitazone, and two days after (Day 5) to regular DMEM medium described above. Experiments were performed on day 7. Upon differentiation, for AMPK activation cells were treated with 2,5 µM AICAR (Sigma Aldrich, A9978) in DMSO for 18h in DMEM high glucose growth media. For bortezomib (BTZ) treatment, upon differentiation, cells were treated with 1nM BTZ (Cell Signaling, 2204S) in DMSO for 18h in DMEM high glucose growth media. For control, equal volume of DMSO was used. The final DMSO concentrations were 0.0125% for the AICAR treatment and 0.01% for the BTZ treatment.

RNA Isolation and Quantitative Real-Time PCR Analysis

Total RNA was isolated from Sirt3 WT and Sirt3 KO adipocytes of both sexes using an NucleoSpin RNA, Mini kit for RNA purification (Machrey-Nagel, Düren, Germany), according to the manufacturer's instructions. Total of 1 µg of RNA was transcribed into cDNA with a High-Capacity cDNA Reverse Transcription Kit (Applied Biosystems, Massachusetts, USA). A quantitative polymerase chain reaction (qPCR) was performed using specific Taqman assays (Supplemental Table S1) and Taqman Gene Expression Master Mix (Applied biosystems, Massachusetts, USA) on 7300 Real-Time PCR System (Applied biosystems, Massachusetts,

USA). The cycling conditions included: an initial incubation at 50°C for 2 minutes, followed by a denaturation step at 95°C for 10 minutes, followed by 40 cycles, consisting of denaturation at 95°C for 15 seconds, annealing and extension at 60°C for 1 minute. Data were analysed using the $2^{-\Delta\Delta Ct}$ method and presented as the fold change in gene expression normalised to the endogenous reference gene β-actin and relative to the corresponding undifferentiated MEF control. β-actin Ct values were comparable across the analysed cell cultures and experimental conditions. All reactions were carried out in triplicate.

Protein Isolation and Western Blot Analysis

After seven days of differentiation, cells were collected using RIPA buffer (50 mM Tris buffer, 150 mM NaCl, 0.1% SDS, 12 mM Na-deoxycholate, 1% Triton) supplemented with protease inhibitors (cOmplete™ EDTA-free EASYpack, Roche, Switzerland) and phosphatase inhibitors (PhosSTOP™ EASYpack, Roche, Switzerland). The lysate underwent sonication twice for 20 seconds (80% amplitude; Labsonic, Biotech International Ltd., Delhi, India) and was then centrifuged at 16,000 × g for 20 minutes at 4°C. The supernatant was collected, and protein concentration was determined using the Pierce™ BCA Protein Assay Kit (Thermo Fisher Scientific, MA, USA). Protein samples were prepared in SDS-PAGE loading buffer (100 mM Tris-HCl, pH 6.8, 2% SDS, 20% glycerol, 4% β-mercaptoethanol, 0.5% bromophenol blue) and analyzed via Western blotting. A total of 15 µg protein per 20 µL sample was separated by SDS-PAGE and transferred onto PVDF membranes (Roche, Switzerland). The membranes were blocked for one hour at room temperature using I-Block™ Protein-Based Blocking Reagent (Invitrogen, MA, USA), followed by overnight incubation at 4°C with primary monoclonal antibodies. Afterward, membranes were incubated with a horseradish peroxidase-conjugated secondary antibody for one hour at room temperature. A complete list of primary and secondary antibodies used is provided in Supplemental Table S2. Total

protein normalization was performed using Amido Black staining (Sigma Aldrich, A8181). Immunoblots were visualized with an enhanced chemiluminescence kit (Bio-Rad, CA, USA) and detected using the Alliance 4.7 Imaging System (UVITEC, Cambridge, UK).

Oil Red Staining and Morphological Characterization of Lipid Droplets

Differentiated and undifferentiated MEF were washed with 1 ml of 1X PBS once before fixing for 5 min with 4% paraformaldehyde in PBS at room temperature. After fixation, MEF were washed three times with 1 ml of PBS and once with 60% isopropanol and were completely air-dried. MEF were then stained with Oil Red O (ORO) [6 ORO:4 ddH2O ratio] (Sigma©) for 10 min at RT. Excess stain residue was removed with four ddH_2O washes. Approximately 1 ml of PBS was then added for microscopic visualization. Images were processed at 460x magnification using a 20x objective lens, with transmitted bright-field light (Olympus IX50 inverted microscope). For quantification, ORO stain particles were eluted with 100% isopropanol and analysed using Thermo Scientific™ Varioskan® Flash (Thermofisher, MA, USA) for spectrophotometry readings at 514 nm. Oil red and staining signal intensity were then used to quantify size, area and percentage of lipid droplet area. Cells that contained lipids above a preset threshold value were considered adipocytes. Lipid droplet quantification was performed on four images per group, analyzing over 100 cells per image. Morphological characterization of lipid droplets was done with ImageJ v1.50i software (NIH).

Normalization of Adipocyte-Related Readouts

Because MEF-derived cultures consisted of mixed populations of differentiated adipocytes and undifferentiated cells, differences in adipogenic differentiation efficiency could confound direct comparisons between experimental groups. Therefore, all adipocyte-related readouts, including Western blot and qPCR were normalized to the corresponding Oil Red O staining

signal. As Oil Red O selectively stains lipid droplets in differentiated adipocytes, its signal was used as a proxy for the adipocyte fraction within each culture. This normalization enabled comparisons between groups to reflect changes associated with differentiated adipocytes rather than differences in the proportion of adipocytes present in the cultures. Importantly, adipogenic differentiation efficiency was reproducible across independent experiments, with each MEF line consistently showing a similar degree of differentiation.

Immunocyctochemistry, Fluorescence and Confocal Microscopy

For immunocytochemistry, differentiated and control MEFs were grown on coverslips in 24-well plates. Before fixation with 4% paraformaldehyde for 30 minutes at room temperature, cells were washed with PBS containing Mg^{2+}/Ca^{2+}. After fixation, cells were blocked with 1% BSA in PBS containing Mg^{2+}/Ca^{2+} and 0.1% Triton X-100 for 1 hour at room temperature. Immunostaining was performed separately with primary antibodies against Perilipin 1 (Plin1, Proteintech-27716-1-AP Rabbit 1:400) and acetyl-CoA carboxylase 1 (Acc1, Proteintech-67373-1-Ig 1:1000) overnight. The following day, the cells were washed three times with PBS Mg^{2+}/Ca^{2+} before incubation with the secondary antibodies (Alexa Fluor 488 anti-rabbit 1:1000 for Plin1 (Invitrogen, A11001), and Alexa Fluor 488-conjugated goat anti-mouse IgG (H+L) 1:1000 for Acc1 (Invitrogen, A11012) for 1 hour in dark at room temperature. After secondary antibody incubation, the cells were washed three times with PBS Mg^{2+}/Ca^{2+}. Oil Red O (ORO) working solution [6 parts ORO: 4 parts ddH_2O] (Sigma©) was then added and incubated for 15 minutes at room temperature. After ORO staining, the cells were washed five times with PBS, followed by DAPI staining (1:100 dilution from stock solution in PBS Mg^{2+}/Ca^{2+}) for 2 minutes in the dark. After a final wash with PBS, the cells were mounted using Dako Aqueous Mounting Medium (Agilent Technologies, Waldbronn, Germany) and viewed with a laser scanning confocal microscope (Plin1), Leica SP8 X FLIM (Leica, Wetzlar,

Germany), and a NIS-Elements AR imaging system on a Nikon Eclipse Ti2 inverted microscope (Nikon Instruments, NY, USA), followed by image acquisition and analysis using NIS-Elements AR software version 6.20.01 (64-bit).

Total Lipid Extraction and Gas Chromatography Analysis

Total lipids were extracted from dried cell pellets using a modified Folch method [18]. Briefly, 5 mL of chloroform was added to each sample and homogenized thoroughly. Subsequently, 1.5 mL of an aqueous $MgCl_2$ solution (0.034%, w/v) was added, followed by vortexing and centrifugation. The upper aqueous phase was carefully removed, and 2.5 mL of 2 M KCl in methanol (4:1, v/v) was added. After vortexing and centrifugation, the aqueous phase was discarded, and 2.5 mL of chloroform/methanol (2:1, v/v) was added. The organic (hydrophobic) phase was collected, transferred to a clean tube, and the solvent was evaporated under a stream of nitrogen. For fatty acid methyl ester (FAME) preparation, lipid extracts were transesterified using 0.5M KOH in methanol for 10 minutes at room temperature. The resulting FAMEs were extracted with n-hexane and analyzed by gas chromatography (GC). GC analysis was performed using a Varian 450-GC system equipped with a flame ionization detector (FID) and a Stabilwax capillary column (crossbond carbowax polyethylene glycol, 60 m × 0.25 mm). Helium was used as the carrier gas. The oven temperature was programmed from 150°C to 250°C at a rate of 5°C/min. Fatty acid methyl esters were identified by comparison of their retention times with those of a commercial standard mixture (Marine Oil FAME Mix, Restek Corporation, Bellefonte, PA, USA). Quantification was based on peak area integration, and the relative abundance of each fatty acid was expressed as a percentage of the total fatty acid content.

LC-MS Metabolomics

All solvents used for the metabolomic analysis were of LC–MS grade. The chemicals were acquired from Sigma-Aldrich Chemical Co. (St. Louis, MO, USA), with the exception of the API-TOF reference mass solution kit (Agilent Technologies, Waldbronn, Germany). Sample preparation and metabolite extraction were performed as described previously [19]. 10 µL of each sample was mixed together to obtain quality control samples (QCs). These QCs, together with blank samples (ACN to water ratio 3:1), were processed the same way as the rest of the samples. An Agilent Technologies Series 1200 binary solvent delivery system (Agilent Technologies, Waldbronn, Germany), coupled to an Agilent 6520 Accurate-Mass Q-TOF detector was used for the LC-ESI-QTOF-MS analysis to obtain the metabolic profile of the plasma samples. A volume of 10 µL for each sample was injected into a reversed-phase column (Discovery® HS C18 HPLC Column, 515 cm × 2.1 mm, 3 µm; Supelco, Bellefonte, PA, USA). The LC-MS method parameters were set as described in [19]. The samples were analyzed in negative ESI mode (full-scan ranging from 50 to 1000 m/z), with a scan rate of 1.02 scans/s. Two reference masses were infused during the analysis for a constant mass correction: 112.9855 (TFA(NH4), detected m/z [C2O2F3(NH4)-H]−) and 966.0007 (HP+FA, detected m/z [C18H18O6N3P3F24+FA-H]−). The Agilent MassHunter 10.0 software (Agilent Technologies, Waldbronn, Germany) was used for the filtering, peak detection, alignment, and integration, as described in details in [19]. The Molecular Feature Extraction (MFE) technique was used for deconvolution of the LC-MS data, and the Recursive Feature Extraction (RFE) algorithm was applied for a second deconvolution step. To assign tentative metabolite candidates, the CEU Mass Mediator search tool was used to assess the list of statistically significant correct masses [20]. The online tool Metaboanalyst version 6.0 (https://www.metaboanalyst.ca/) was used to apply a multivariate statistical analysis [21]. The data matrix was normalized by sum, log-transformed and pareto-scaled prior to a partial

least squares-discriminate analysis (PLS-DA) for the variable importance estimation. Based on the PLS-DA models, the variable importance in projection (VIP) scores were acquired.

Transmission Electron Microscopy

Upon treatment, cell pellets were immediately fixed with a 2.5 % glutaraldehyde (Agar Sci, Essex, UK) in 0.2 M phosphate buffer (PB) for 4 h at 4°C. After fixation cells were rinsed 3 times in 0.1 M PB, embedded in agar and postfixed in 1 % osmium tetroxide in the same buffer. Samples were dehydrated in a graded series of ethanol and embedded in resin (Agar Sci, Essex, UK). In total, 20 resin blocs were cut with diamond knife (Diatome, Agar Sci, Essex, UK) with Ultracut UC6 ultramicrotome (Leica Microsystems, Wetzlar, Germany), into 80- to 100-nm thin sections and analysed with CM12 transmission electron microscope operated at 80 kV (Philips/FEI, Eindhoven, Netherlands), equipped with a digital camera (SIS MegaView III, Olympus Soft Imaging Solutions, Münster, Germany).

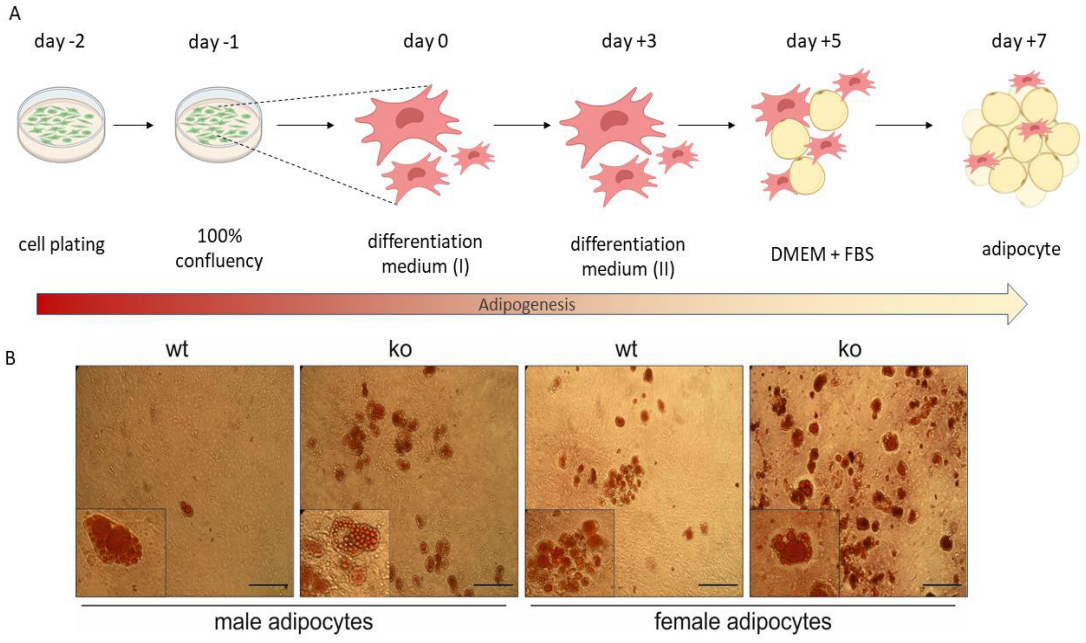
Statistical Analysis

SPSS Statistics 23.0 (IBM, USA) was used for statistical data analysis. Before performing the analyses, the normality of the sample distribution was assessed using the Shapiro–Wilk test. For normally distributed samples, a two-way ANOVA was conducted to examine the interaction effect of two factorial variables. When a significant interaction was observed, a Bonferroni adjustment was applied to correct for multiple comparisons within each simple main effect separately. Statistical significance was set at $p < 0.05$.

Results

Sirt3 Loss Promotes Lipid Droplet Accumulation and Enlargement in Female Adipocytes

We differentiated WT and Sirt3 KO MEFs of both sexes (hereafter WT and KO, respectively) into MEF-derived adipocytes (hereafter adipocytes) according to a published protocol with minor modifications [9] (Figure 1A). To assess the success of the differentiation, we analysed lipid droplet accumulation in the differentiated cells using Oil Red O staining. All groups were positive for lipid droplets after induction with the differentiation medium, whereas control cells did not accumulate any lipids (Figure 1B, 1C, Supplementary Fig. S1). Among differentiated adipocytes, the KO group accumulated more lipid droplets than the WT group in both sexes, with lipid accumulation being most pronounced in female KO adipocytes. Confocal imaging and quantitative analysis showed that the absence of Sirt3 altered lipid droplet (LD) morphology and abundance in a sex-dependent manner, with female KO adipocytes displaying both a higher number and a larger size of LDs compared with males (Figure 1D–F) and confirmed that control cells did not accumulate lipids (Supplementary Fig. S2).



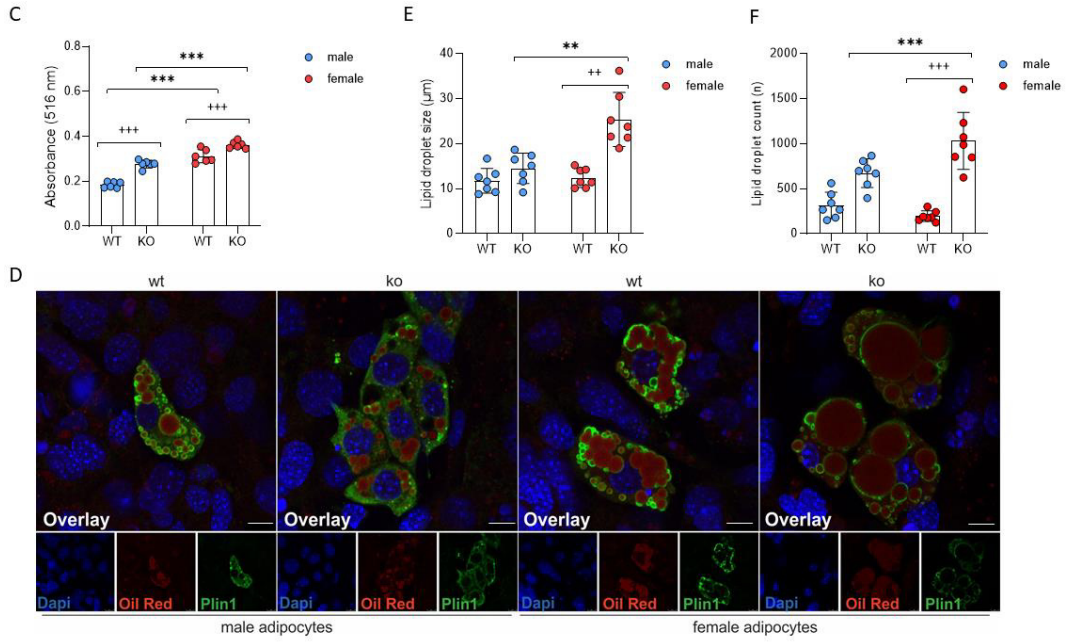


Figure 1. Female KO adipocytes exhibit the highest lipid droplet accumulation and enlargement (A) *Schematic illustration of experimental workflow of MEF-derived adipocyte differentiation process in vitro. Differentiation medium (I) - insulin, rosiglitazone, IBMX, dexamethazone; differentiation medium (II) - insulin, rosiglitazone. DMEM - Dulbecco's Modified Eagle Medium; FBS - Fetal Bovine Serum.* ***(B)*** *Oil Red O staining of lipid droplets in a population of adipogenically differentiated MEF (adipocytes) after 7 days of differentiation. Scale bar: 100 µm; magnification is 10x. Inset image: magnification is 40x. The inset images are magnified four times to highlight lipid morphology. A representative image is shown.* ***(C)*** *Graphical representation of spectrophotometric quantification of Oil Red O staining in adipocytes after 7 days of differentiation. a.u., arbitrary units.* ***(D)*** *Representative confocal images of differentiated adipocytes. Blue (DAPI) – nuclear staining; red (Oil Red) – lipid droplet staining; green (Plin-1) – lipid droplet-associated protein staining. The white scale bar corresponds to 10 µm.* ***(E)*** *Quantification of lipid droplet diameter and* ***(F)*** *lipid droplet count in differentiated cells using software ImageJ. Data were analyzed by two-way ANOVA followed*

*by post-hoc test with Bonferroni adjustment; $^{+++}p<0.001$, $^{++}p<0.01$, WT vs. KO; ***p<0.001, **p<0.01, male vs. female. For each group, seven images were analyzed. Data are presented as mean ± SD.*

Next, we assessed the expression of specific adipogenic markers using quantitative polymerase chain reaction (qPCR) (Figure 2). On day 7 of differentiation, *Ppar-γ, Fabp4,* and *Adipoq* expression was increased in differentiated cultures compared with their undifferentiated controls, indicating activation of the adipogenic transcriptional programme in MEF-derived adipocyte cells. Gene expression analysis showed that *Ppar-γ*, *Adipoq*, and *Fabp-4* were increased after differentiation, with generally higher expression in female than male adipocyte cultures and the highest levels observed in KO female adipocytes (Figure 2).

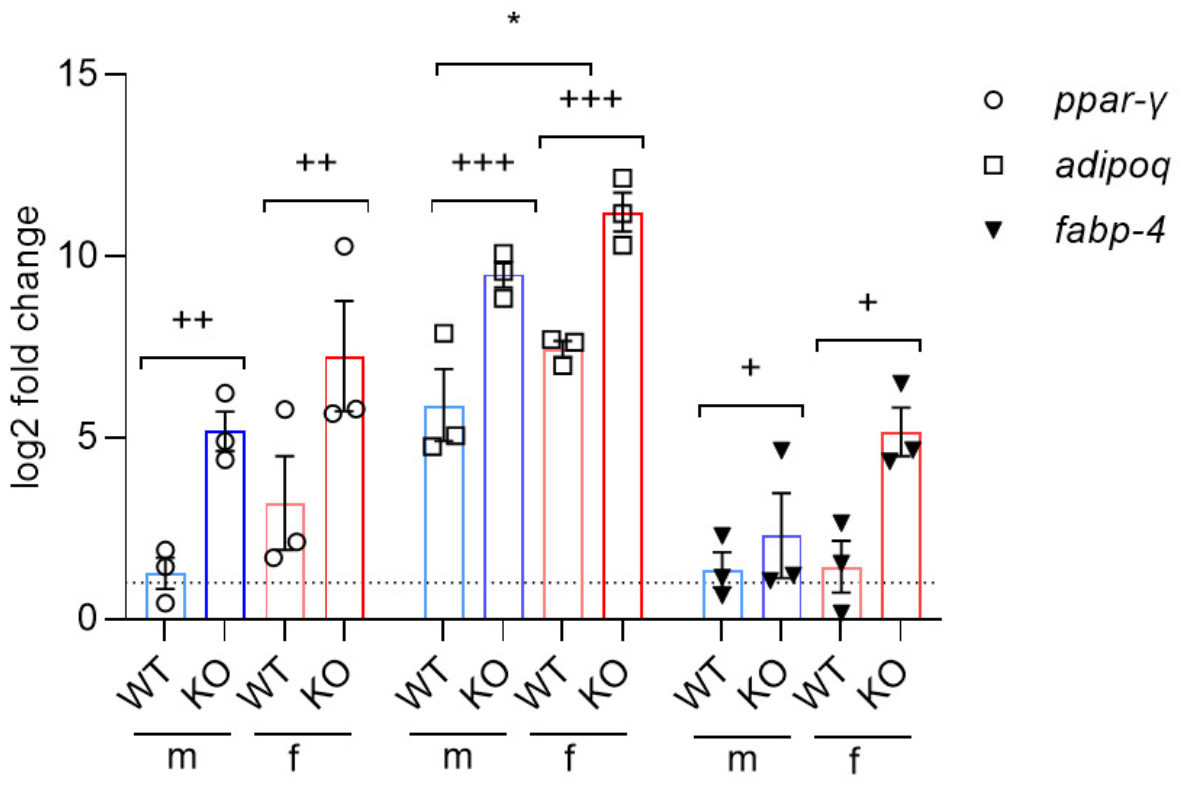


Figure 2. Female KO adipocytes show the strongest induction of adipogenic gene expression. *Gene expression of Ppar-γ, Adipoq, and Fabp-4 in differentiated WT and Sirt3 KO MEF-derived*

adipocytes of both sexes. RT-qPCR data were normalized to Oil Red O staining to correct for differences in adipocyte abundance across experimental groups and are shown as log2 fold change relative to the corresponding undifferentiated controls, indicated by the dotted line at y = 1. Data are presented as mean ± S.E.; individual points represent independent biological experiments. Data were analyzed by two-way ANOVA followed by Bonferroni-adjusted post hoc comparisons. $^{+++}p < 0.001$, $^{++}p < 0.01$, $^{+}p < 0.05$, WT vs. KO; $^{*}p < 0.05$, male vs. female.

As previously shown, female adipocytes displayed higher lipid accumulation than male adipocytes, a difference that was further amplified by Sirt3 deficiency. Therefore, we aimed to determine whether this increased lipid accumulation results from differences in key regulators of lipid synthesis and breakdown. Specifically, we analysed the protein expression of Ppar-γ, a key adipogenic factor, Acc1 and Fasn which are involved in *de novo* lipogenesis, and Atgl, an enzyme responsible for lipolytic breakdown, to assess potential imbalances in these metabolic pathways. Protein expression of key lipogenic enzymes was consistent with lipid accumulation in KO female adipocytes. Two-way ANOVA showed strong sex-dependent regulation of Ppar-γ, with female adipocytes displaying reduced expression across genotypes (Figure 3A, 3F). The pAcc1/Acc1 ratio was reduced by Sirt3 loss in both sexes and was consistently lower in females than males, indicating reduced inhibitory Acc1 phosphorylation, particularly in female KO cells (Figure 3B, 3F). Sirt3 loss reduced Fasn in male adipocytes but increased it in female adipocytes, supporting female specific activation of lipogenic signalling in Sirt3-deficient adipocytes (Figure 3C, 3F). Atgl, the enzyme that initiates lipolysis, was markedly reduced by Sirt3 loss in female adipocytes but not in males, indicating a female specific impairment of lipolytic capacity in Sirt3 KO adipocytes (Figure 3D, 3E, 3F).

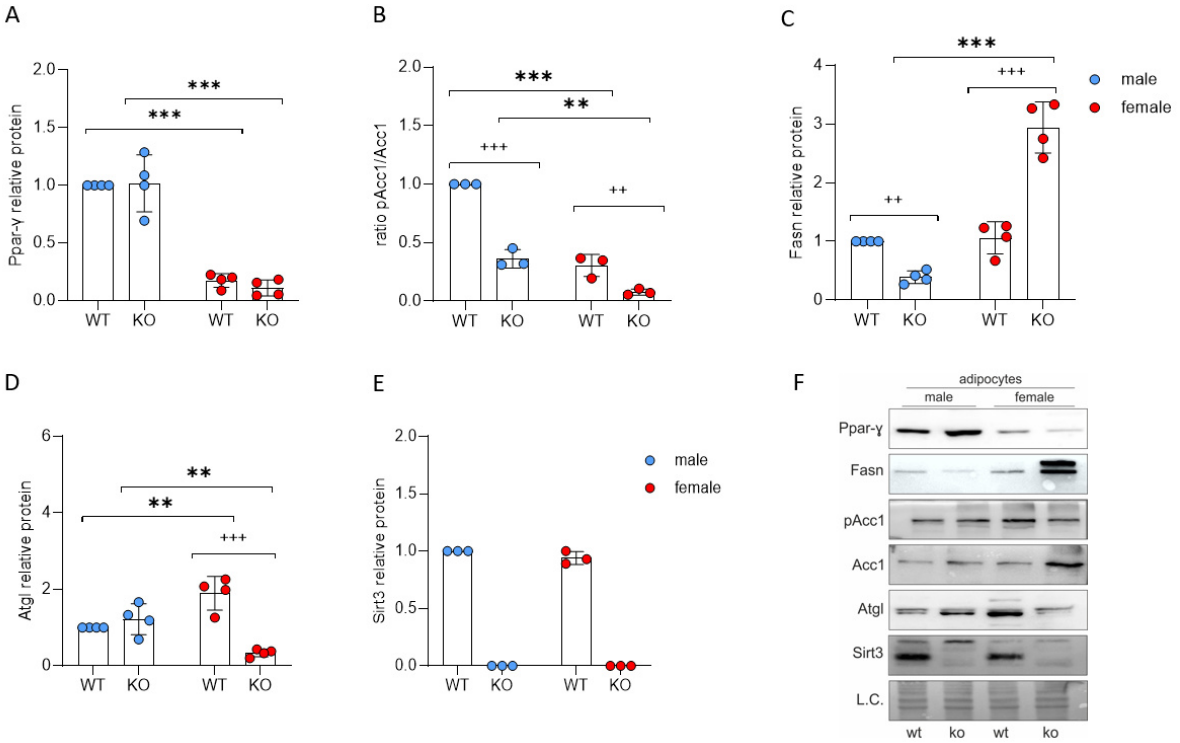


Figure 3. Sirt3 loss promotes female-specific de novo lipogenesis and reduces lipolysis. *Immunoblot analysis of key regulators of lipid metabolism in male and female WT and KO adipocytes.* ***(A)*** *Ppar-γ,* ***(B)*** *pAcc1/Acc1 ratio,* ***(C)*** *Fasn,* ***(D)*** *Atgl,* ***(E)*** *Sirt3,* ***(F)*** *Representative immunoblots for the proteins shown in A–E. L.C., loading control. Data were analyzed by two-way ANOVA followed by post-hoc test with Bonferroni adjustment; $^{+++}p<0.001$, $^{++}p<0.01$, WT vs KO; $^{***}p<0.001$, $^{**}p<0.01$, $^{*}p<0.05$, male vs. female. Data were normalized to Oil Red O staining to correct for differences in adipocyte abundance across experimental groups. N = 3-4 biological replicates per group. Values are presented as mean ± SD.*

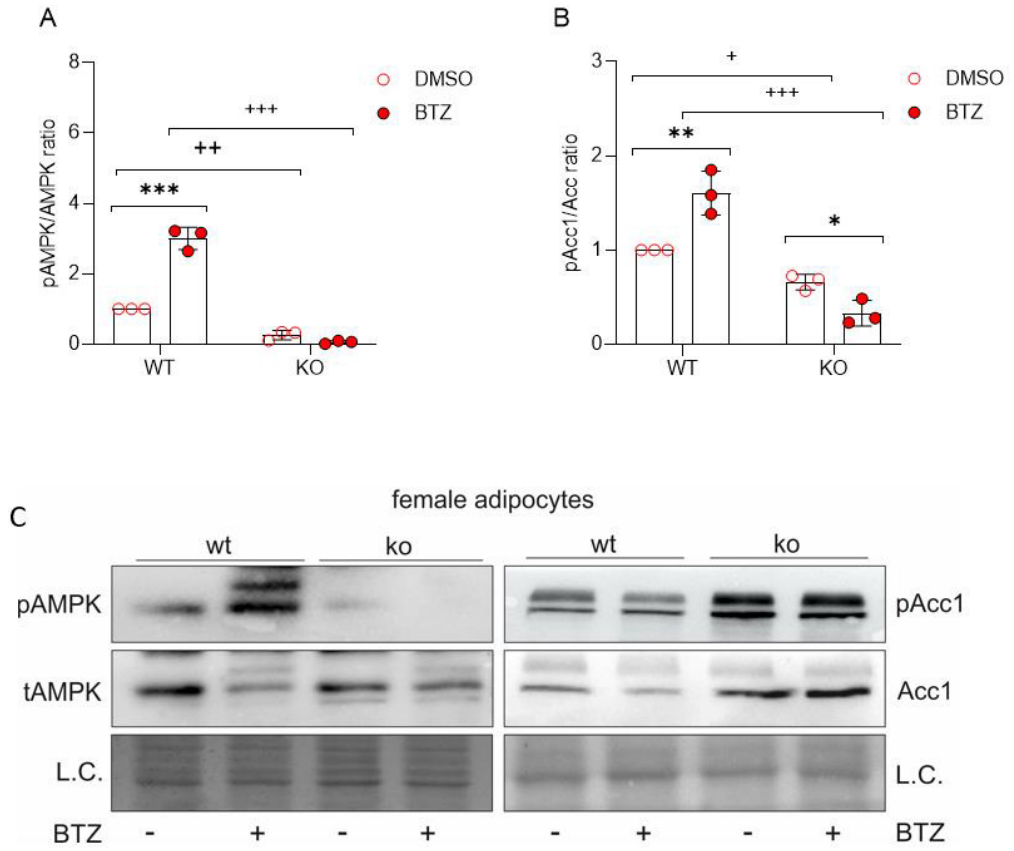
Bortezomib-Induced Lipid Accumulation in KO Female Adipocytes is Linked to Dysregulated AMPK–Acc1 Axis

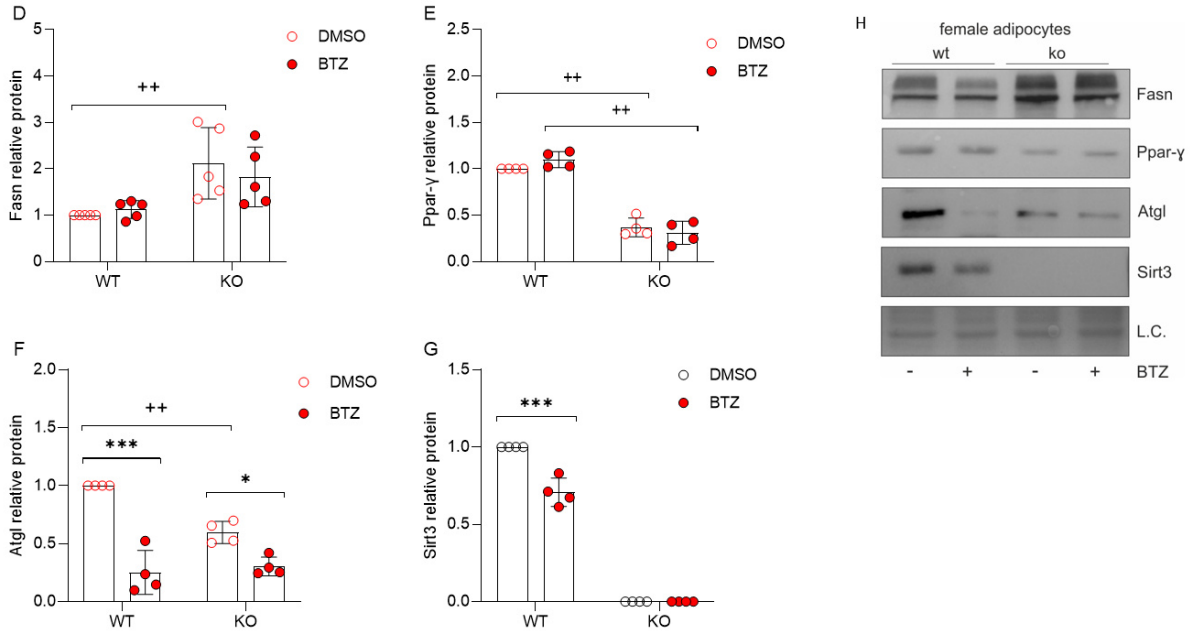
Female-specific enhancement of *de novo* lipogenic signalling in the absence of Sirt3, evidenced by increased Fasn expression, reduced inhibitory phosphorylation of Acc1, and decreased Atgl expression, suggests an imbalance between lipid synthesis and breakdown.

Given that AMPK restrains *de novo* lipogenesis via Acc1 phosphorylation [22] and that Sirt3 supports AMPK activation [23], we next tested whether loss of Sirt3 disrupts AMPK–Acc1 signalling, a central pathway governing lipid metabolism. o investigate this, we used bortezomib (BTZ), a proteasome inhibitor reported to activate AMPK and suppress lipogenic gene expression, including Srebp-1c, Fasn, and Acc1 [24, 25], to determine whether Sirt3 deficiency compromises the AMPK–Acc1 antilipogenic response and thereby promotes lipid accumulation. As female adipocytes exhibited the greatest lipid accumulation, which was further amplified by Sirt3 loss, subsequent experiments were performed exclusively in female adipocytes.

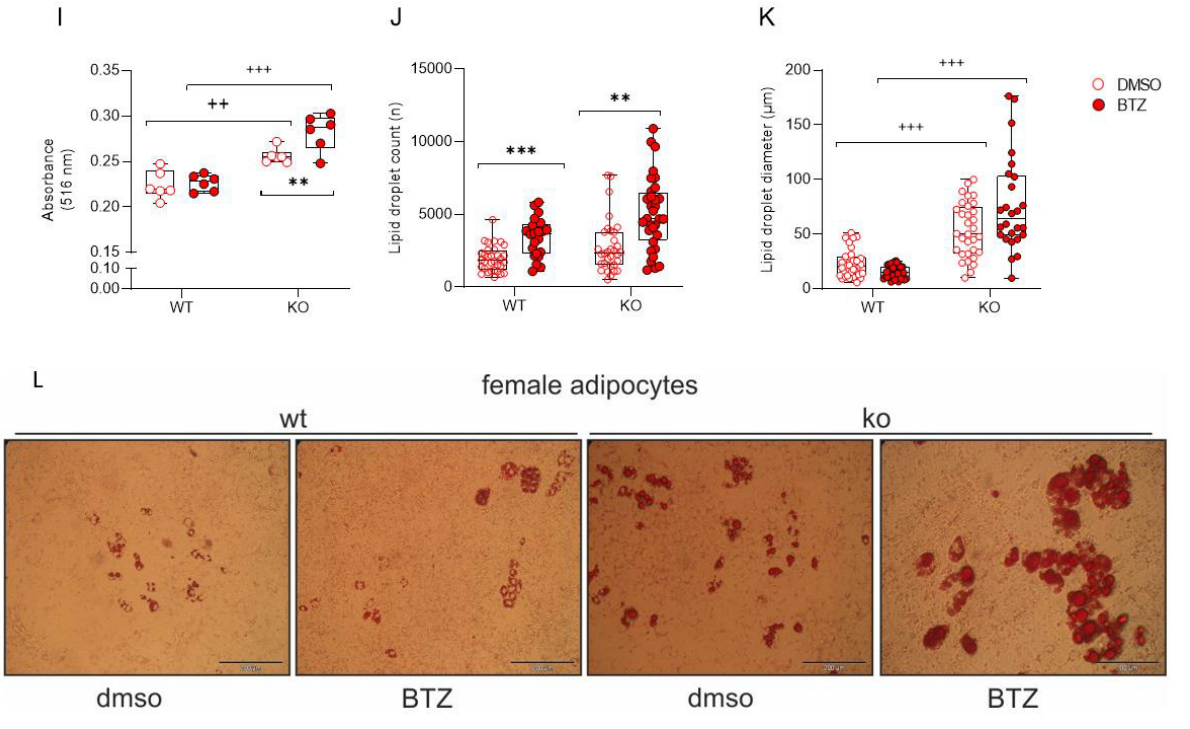
BTZ strongly activated AMPK in WT adipocytes, as indicated by a significant increase in the pAMPK/AMPK ratio. This was accompanied by a rise in the pAcc1/Acc1 ratio, consistent with Acc1 inactivation and suppression of *de novo* lipogenesis, thereby confirming its antilipogenic effect (Fig. 4A–C). In contrast, KO adipocytes exhibited a significantly lower basal pAMPK/AMPK ratio, with complete loss of the signal upon BTZ treatment, resulting in an absence of AMPK activation compared with WT cells. Furthermore, despite treatment, Acc1 remained active in KO adipocytes, as evidenced by a decreased pAcc1/Acc1 ratio, suggesting a metabolic shift towards lipogenesis. These results indicate that Sirt3 mediates BTZ-induced AMPK–Acc1 activation, promoting inhibitory phosphorylation of Acc1 and limiting *de novo* lipogenesis. In parallel with low pAMPK/AMPK and pAcc1/Acc1 ratios, KO cells displayed high Fasn protein expression, further supporting enhanced *de novo* lipogenesis, whereas this genotype difference was no longer significant after BTZ treatment (Fig. 4D–H). High magnification immunofluorescence imaging was used to qualitatively assess Acc1 localization and showed that Acc1 signal was detectable in Oil Red O-positive adipocyte-like cells, with apparent enrichment near lipid droplet-associated regions (Supplementary Fig. S3).

Quantification of Oil Red O staining, lipid droplet number, and lipid droplet diameter collectively shows that Sirt3 deficiency markedly enhances lipid accumulation in female adipocytes, and that BTZ treatment further accentuates this phenotype (Fig. 4I–L). KO adipocytes exhibited significantly higher ORO absorbance and substantially enlarged droplet size compared with WT cells under both control and BTZ-treated conditions. While BTZ induced a modest increase in lipid storage in WT adipocytes, its effect was considerably stronger in KO cells, resulting in the largest and most numerous lipid droplets. Collectively, these findings indicate that loss of Sirt3 impairs the AMPK–Acc1 response to BTZ, thereby limiting the antilipogenic effect of proteasome inhibition and leading to pronounced lipid accumulation following BTZ exposure.





396



397

398 ***Figure 4. Sirt3 loss abolishes BTZ-induced AMPK–Acc1 activation and exacerbates lipid***

399 ***accumulation in female adipocytes*** *Immunoblot analysis of key proteins of lipid metabolism*

400 *and Oil Red O staining of lipid droplets after BTZ treatment in differentiated female WT and*

401 *KO adipocytes.* ***(A)*** *pAMPK/AMPK ratio,* ***(B)*** *pAcc1/Acc1 ratio,* ***(C)*** *representative immunoblots*

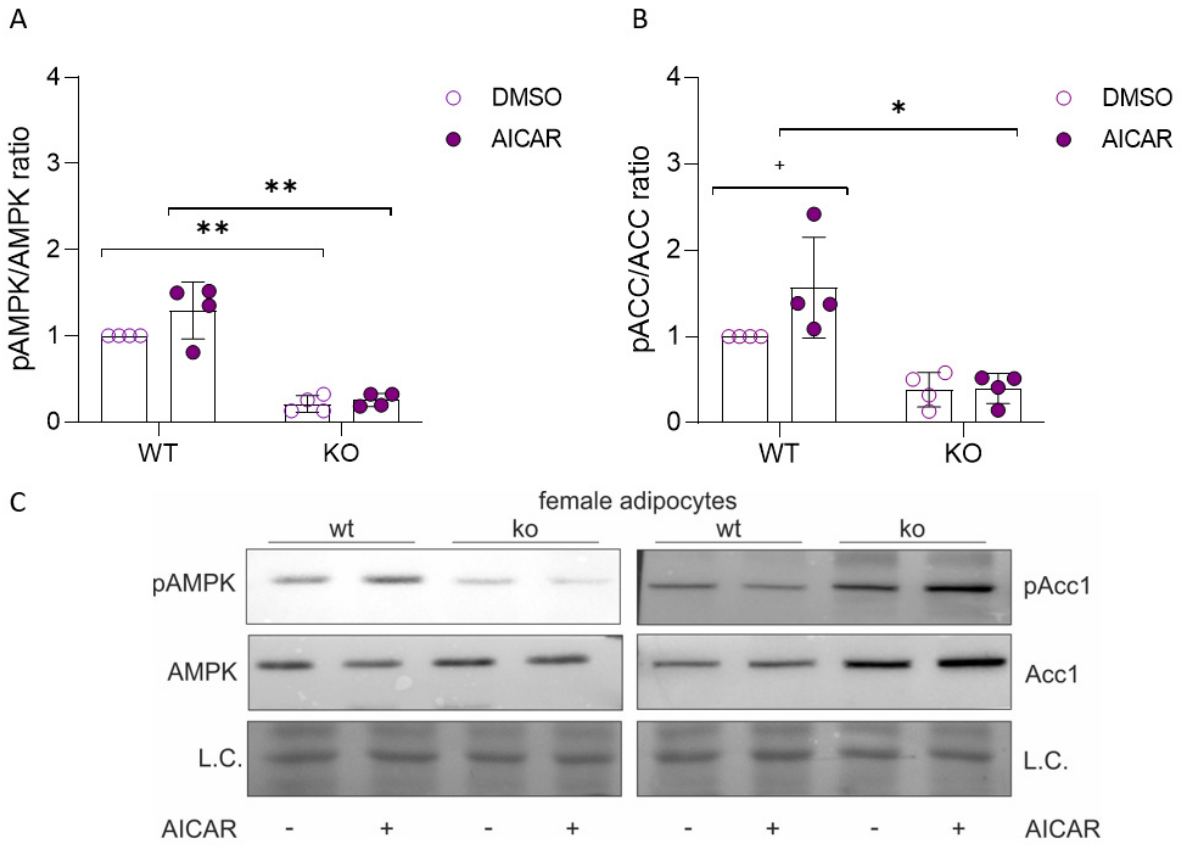
402 *for the proteins shown in A and B,* ***(D)*** *Fasn,* ***(E)*** *Ppar-γ,* ***(F)*** *Atgl,* ***(G)*** *Sirt-3,* ***(H)*** *representative*

immunoblots for the proteins shown in D-G. L.C., loading control. Data were analyzed by two-way ANOVA followed by post-hoc test with Bonferroni adjustment; n = 3-5 biological replicates per group. Data were normalized to Oil Red O staining to correct for differences in adipocyte abundance across experimental groups. Values are presented as mean ± SD. ***(I)*** *Graphical presentation of Oil Red O absorbance and staining of lipid droplets in female WT and KO adipocytes after bortezomib treatment. Absorbance at 516 nm. Lipid droplet count* ***(J)****, lipid droplet size* ***(K)****. Two-way ANOVA was used followed by post-hoc test with Bonferroni adjustment or Kruskal–Wallis nonparametric ANOVA followed by Dunn's post hoc test for multiple comparisons. ***p<0.001, **p<0.01, *p<0.05 DMSO vs. bortezomib; $^{+++}$p<0.001, $^{++}$p<0.01, $^{+}$p<0.05 WT vs. KO.* ***(L)*** *Representative microscopic images of Oil Red O staining of lipid droplets in female WT and KO adipocytes after BTZ treatment. For each group three independent biological replicates were analyzed. From each replicate, five wells were imaged, with 5 to 6 images acquired per well. Scale bar: 200 µm.*

Sirt3 Is Required for AMPK Activation by AICAR in female adipocytes

To directly test whether Sirt3-deficient female adipocytes have an intrinsic inability to activate AMPK, we examined their response to AICAR, a well-established pharmacological AMPK activator. AICAR treatment did not significantly affect the pAMPK/AMPK ratio, whereas Sirt3 genotype had a strong effect, with markedly lower pAMPK/AMPK levels in KO than WT adipocytes irrespective of treatment (Fig. 5A, C). The pAcc1/Acc1 ratio, calculated from matched normalized pAcc1 and total Acc1 values, was significantly affected by Sirt3 genotype, with markedly lower values in KO than WT adipocyte cultures irrespective of AICAR treatment; AICAR itself did not significantly increase this ratio (Fig. 5B, C). Together, these findings indicate that Sirt3 deficiency is associated with a persistent impairment of the AMPK–Acc1 signalling axis, suggesting a reduced capacity of KO adipocytes to activate antilipogenic

phosphorylation pathways even upon pharmacological AMPK stimulation. Oil Red O staining confirmed that Sirt3 deficiency itself drives excessive lipid accumulation in female adipocytes, as both KO DMSO and AICAR groups exhibited significantly higher lipid content than their WT counterparts. AICAR treatment did not alter lipid storage in KO cells, indicating that pharmacological activation of AMPK is insufficient to overcome the metabolic defect caused by Sirt3 loss (Fig. 5D, E). Collectively, these results suggest that impaired AMPK–Acc1 signalling underlies lipid accumulation in KO adipocytes, and that this phenotype cannot be rescued by either proteasome inhibition or direct AMPK activation.



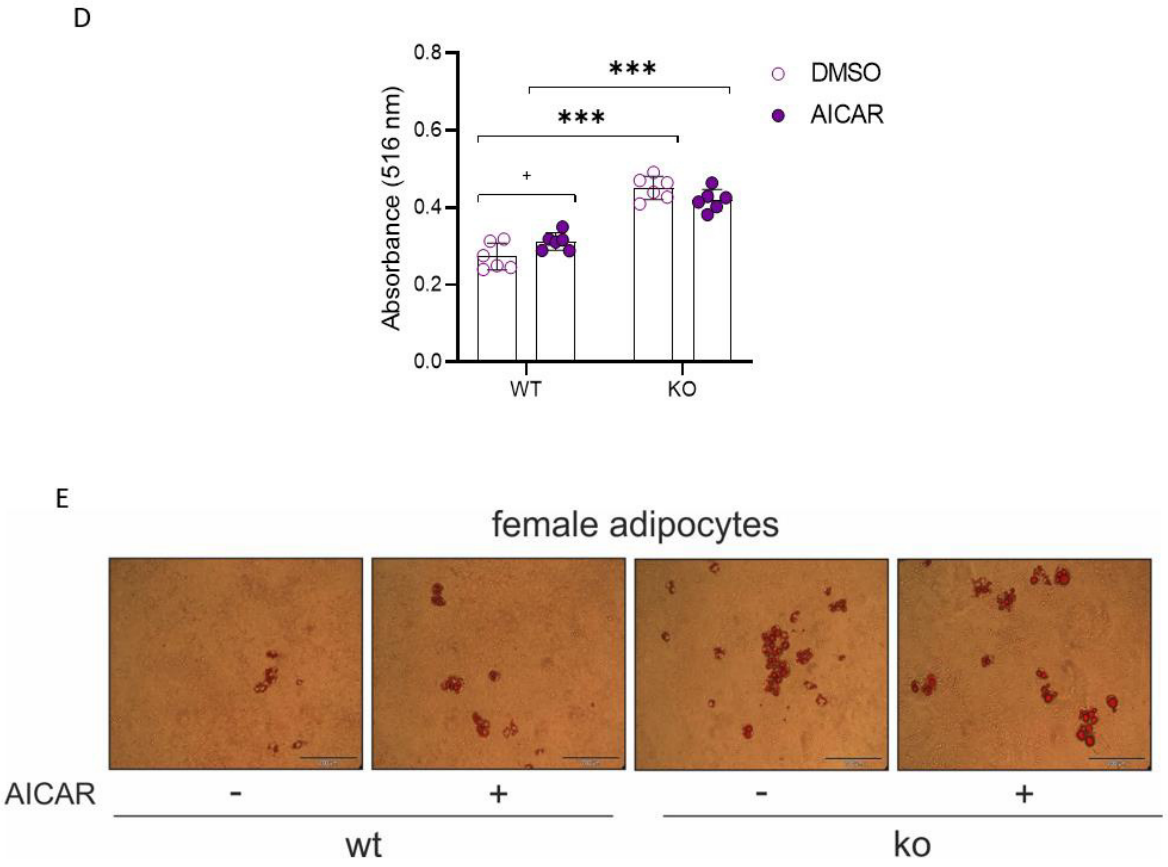


Figure 5. Sirt3 is required for AICAR-responsive AMPK–Acc1 signaling and control of lipid accumulation. *Graphical display of* ***(A)*** *pAMPK/AMPK ratio,* ***(B)*** *pAcc/Acc ratio,* ***(C)*** *representative immunoblots for the proteins shown in A and B. Data were analyzed by two-way ANOVA followed by post-hoc test with Bonferroni adjustment. Data were normalized to Oil Red O staining to correct for differences in adipocyte abundance across experimental groups. N = 4 biological replicates per group.* ***(D)*** *Graphical presentation of Oil Red O absorbance in female WT and KO adipocytes after AICAR treatment. ***p<0.001, **p<0.01, WT vs. KO; $^{+}$p<0.05, DMSO vs. AICAR.* ***(E)*** *Representative microscopic images of Oil Red O staining of lipid droplets in female WT and KO adipocytes after AICAR treatment. For each group three independent biological replicates were analyzed. From each replicate, five wells were imaged, with five to six images acquired per well. Scale bar: 200 µm.*

Sirt3 Loss Promotes Scd1-Associated Fatty Acid Desaturation In Female Adipocytes

To further characterise the lipid-accumulating phenotype of KO adipocytes, we quantified the palmitoleate-to-palmitate desaturation index (C16:1/C16:0), a commonly used surrogate marker of Scd1-dependent Δ9 desaturation [26, 27]. The C16:1/C16:0 ratio was significantly higher in KO than WT adipocytes, indicating enhanced palmitate-to-palmitoleate desaturation in the absence of Sirt3. BTZ treatment modestly reduced the ratio across groups; however, KO adipocytes maintained higher values than WT cells under both control and BTZ-treated conditions (Fig. 6A, Supplementary Fig. S4A,B). Consistently, western blot analysis showed markedly increased Scd1 protein abundance in KO compared with WT adipocytes, while BTZ significantly reduced Scd1 protein abundance in KO cells but had no detectable effect in WT cells (Fig. 6B, C). Together, these results indicate that Sirt3 deficiency promotes an Scd1-associated desaturation phenotype, whereas BTZ reduces Scd1 protein abundance without fully reversing the elevated C16:1/C16:0 ratio in KO adipocytes. Together, these results indicate that Sirt3 deficiency increases Scd1-associated desaturation, while BTZ reduces Scd1 protein abundance in KO adipocytes without normalizing the elevated C16:1/C16:0 ratio.

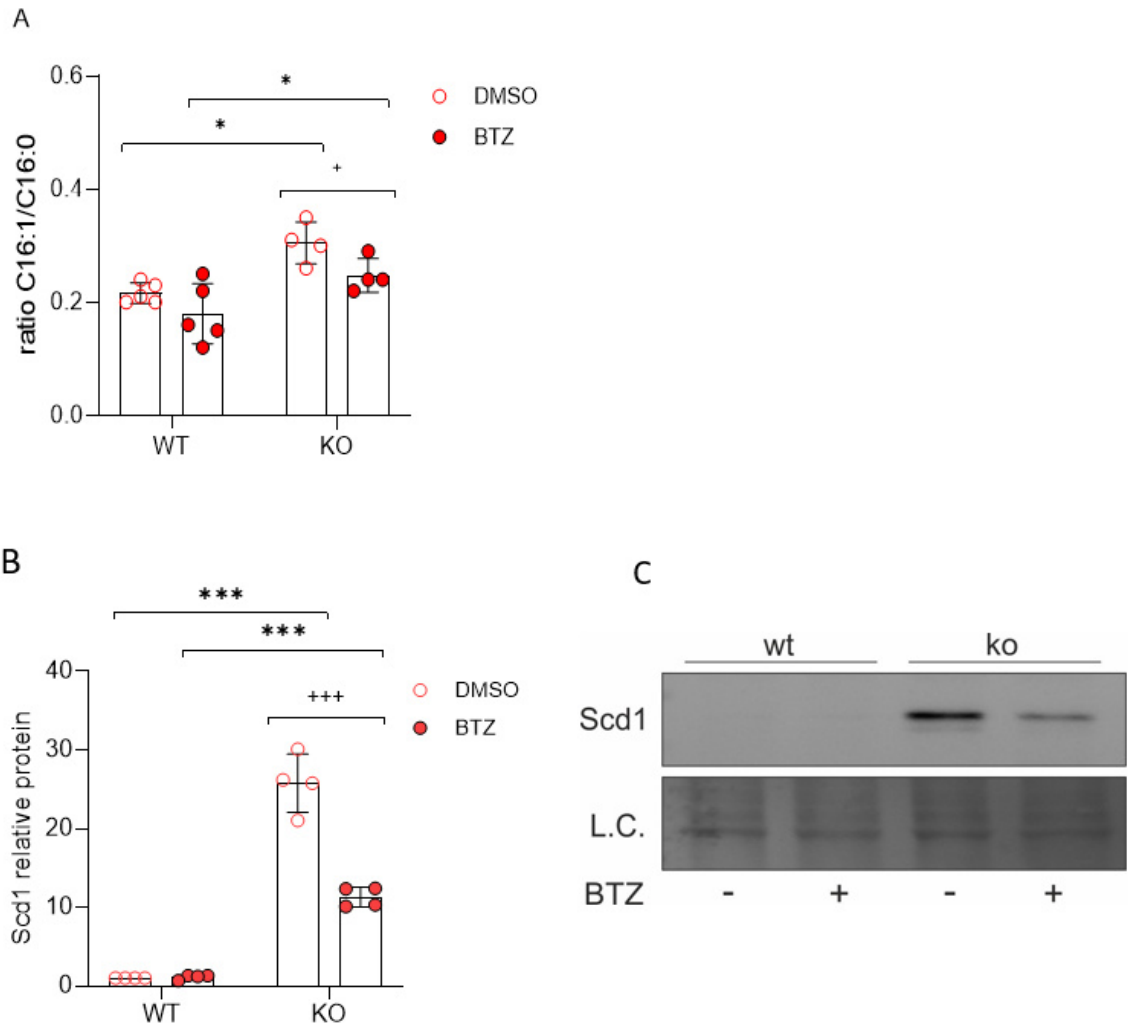


Figure 6. Sirt3 loss enhances Scd1-associated fatty acid desaturation in adipocytes. (A) *Palmitoleate to palmitate ratio (C16:1/C16:0), used as an index of Scd1-dependent Δ9-desaturation, in WT and KO adipocytes treated with DMSO or BTZ.* ***(B)*** *Relative protein expression of Scd1 in WT and KO adipocytes under DMSO and BTZ-treated conditions.* ***(C)*** *Representative immunoblots of Scd1. L.C., loading control. Data were analyzed by two-way ANOVA followed by post-hoc test with Bonferroni adjustment and normalized to Oil Red O staining to correct for differences in adipocyte abundance across experimental groups. ***p<0.001, *p<0.05, WT vs. KO; $^{+++}$p<0.001, $^{+}$p<0.05, DMSO vs. BTZ. N = 4-5 biological replicates per group. Values are presented as mean ± SD.*

BTZ induces genotype-independent remodeling of glycerophospholipid and lysophospholipid profiles

To further characterise the metabolic response to BTZ treatment, LC–MS-based metabolomic profiling was performed in both positive and negative ionisation modes. PLS-DA analysis revealed clear separation between DMSO- and BTZ-treated cells in both WT and KO adipocytes, with the corresponding score plots shown in Fig. 7A–D. To identify the metabolites contributing most strongly to this separation, VIP scores were calculated from the PLS-DA models, and the top 10 metabolites in each ionisation mode are shown in Supplementary Fig. S5A–D. Across both genotypes, the highest-ranking predictor metabolites predominantly belonged to glycerophospholipid and lysophospholipid classes, indicating that BTZ-induced metabolic perturbations extend to membrane lipid remodelling pathways.

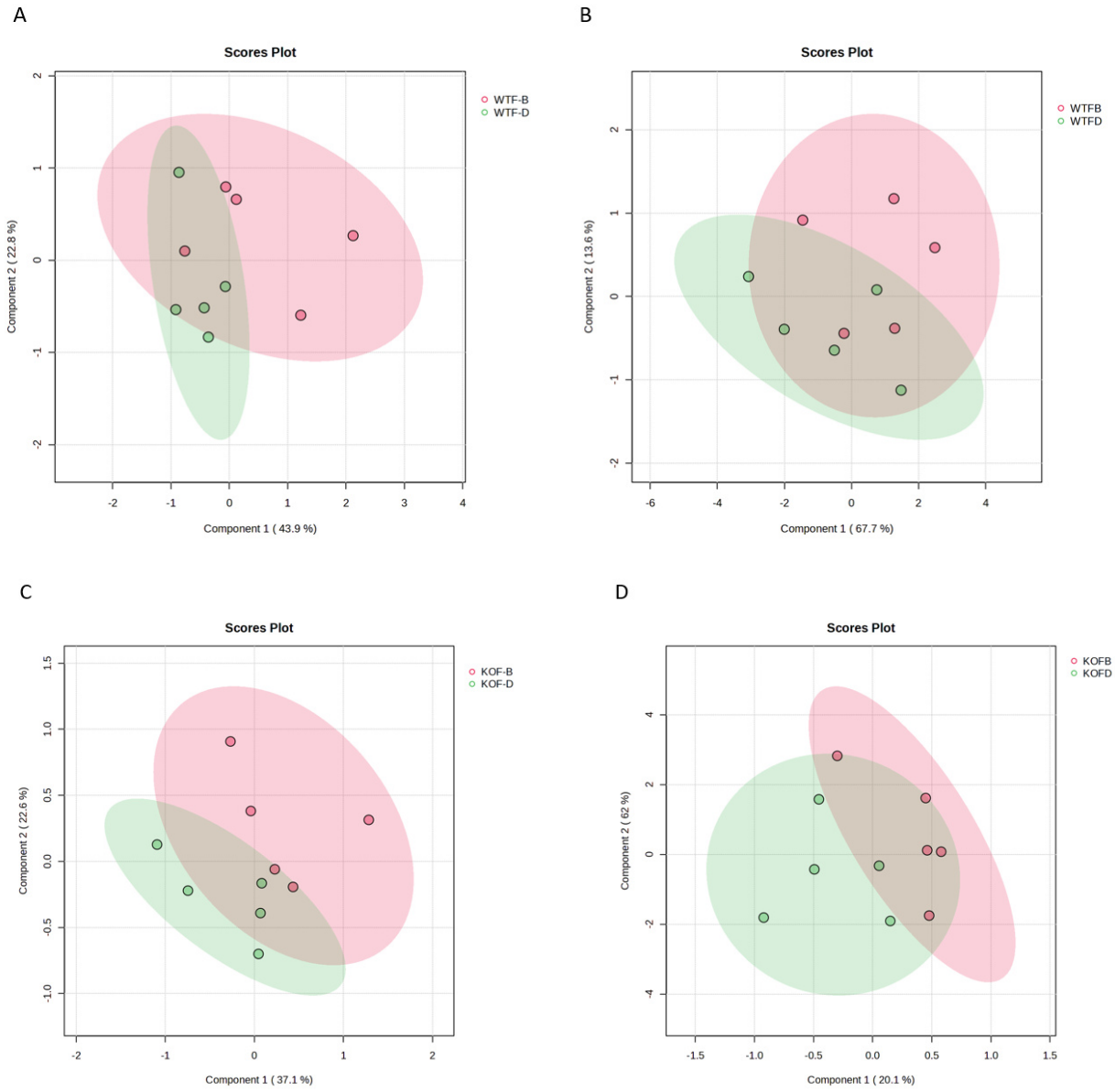


Figure 7. *PLS-DA score plots showing separation between control (green) and bortezomib-treated (red) groups in WT adipocytes in (A) negative and (B) positive ion mode, and in KO adipocytes in (C) negative and (D) positive ion mode. Elipses represent 95 % confidence intervals for each individual group. N=4–5 technical replicates per group.*

In WT cells, key discriminant metabolites included multiple phosphatidylethanolamine (PE), phosphatidylglycerol (PG), phosphatidylserine (PS), lysophosphatidylcholine (LPC), and lysophosphatidylserine (LPS) species. In addition to broad alterations in glycerophospholipid turnover (as reflected by changes in PE, PG, and LPC levels), several PS and LPS species (PS

18:0, LPS 18:1, PS P-28:0, PS 30:0, PS 40:0) may indicate activation of phosphatidylserine externalisation and apoptotic signalling pathways. In KO cells, tentative analysis highlighted PE, lysophosphatidylethanolamine (LPE), and PG species as the dominant discriminant metabolites. Although BTZ treatment induced detectable metabolic changes in both genotypes, particularly in glycerophospholipid and lysophospholipid metabolite levels, these alterations did not clearly support impaired AMPK-associated metabolic adaptation or markedly enhanced lipid accumulation in KO adipocytes. The absence of a clear metabolomic signature of impaired AMPK activation in KO cells may indicate compensatory metabolic adaptations or insufficient metabolic divergence under the applied experimental conditions.

Sirt3 Deficiency Enhances BTZ-Associated Lipid Accumulation And Ultrastructural Organelle Stress In Female Adipocytes

To further assess whether the enhanced lipid accumulation observed in female KO adipocytes was accompanied by ultrastructural alterations, we performed qualitative light and transmission electron microscopy analyses. Semithin sections were used as a qualitative morphological complement to the quantitative lipid analyses and illustrated lipid containing adipocyte-like cells under control and BTZ-treated conditions, but were not used to quantify lipid droplet abundance (Supplementary Fig. S6A). Transmission electron microscopy additionally revealed lipid bodies and autophagic structures, with the most evident changes observed in KO cells (Supplementary Fig. S6B). Ultrastructural analysis at higher magnification showed features consistent with endoplasmic reticulum (ER) stress induced by BTZ treatment, including enlargement and vesiculation of the granular ER (gER) in WT cells, whereas KO cells displayed granular structures resembling aggresomes, enlarged rounded mitochondria, and apparent disruption of the close spatial organisation between gER and mitochondria (Supplementary Fig. S6C). These qualitative ultrastructural findings are consistent with a more

pronounced organelle stress response in female KO adipocytes. However, TEM was used here for qualitative ultrastructural assessment and not for quantification of mitochondrial mass or mitochondrial biogenesis.

Discussion

The aim of this study was to investigate the role of Sirt3 in adipogenic processes in the context of biological sex, as both factors contribute to metabolic homeostasis. Using MEF-derived adipocytes as a model system, we found that adipogenic differentiation and lipid storage were influenced by both Sirt3 status and sex. ORO-normalized expression of the adipogenic genes *Ppar-γ*, *Fabp-4*, and *Adipoq* increased after differentiation in all groups, supporting induction of the adipogenic transcriptional program and confirming that MEFs can serve as an adaptive *in vitro* model of adipogenesis [28, 29]. Sirt3 deficiency further enhanced adipogenic marker expression in both sexes, with female KO adipocytes showing the highest overall expression profile, consistent with their pronounced lipid accumulation. These findings are consistent with previous reports linking Sirt3 to the regulation of lipid metabolism, lipogenesis, and lipid uptake [30, 31] and suggest that loss of Sirt3 promotes adipocyte lipid storage in a sex-dependent manner. Consistent with the gene expression data, confocal imaging and lipid droplet morphometry revealed pronounced sex- and Sirt3-dependent differences in lipid droplet organization. Female KO adipocytes showed the highest lipid droplet number and size, indicating that Sirt3 loss particularly enhances lipid storage capacity in female cells. Altered lipid droplet morphology is closely associated with metabolic dysfunction and reflects changes in lipid synthesis, lipid droplet-associated proteins, lipid mobilization, and cellular metabolic state [32, 33]. Thus, the absence of Sirt3

appears to disrupt lipid droplet homeostasis more strongly in female adipocytes, probably through combined effects on lipid synthesis and turnover.

Our previous results have shown that KO MEFs exhibit sex-specific differences in stress adaptation, including Hif-1α stabilization in males, stronger antioxidant responses in females, and differential susceptibility to genotoxic stress [16, 34]. The present findings extend this concept to adipogenic differentiation, indicating that Sirt3 contributes not only to stress adaptation but also to the metabolic remodeling that supports adipocyte maturation and lipid storage capacity. Protein expression analysis further revealed discrepancies between adipogenic transcriptional activation and protein level responses. Although female KO adipocytes showed the highest ORO-normalized adipogenic gene expression profile and lipid accumulation, Ppar-γ protein levels were lower in female than male adipocytes, suggesting that lipid storage in this model is not simply explained by canonical Ppar-γ protein abundance. This may reflect sex-dependent posttranscriptional regulation, altered Ppar-γ activity, or compensatory mechanisms linked to Sirt3 absence [35]. Interestingly, the expression of Atgl, the rate-limiting enzyme in lipolysis, was also regulated in a sex- and Sirt3-dependent manner. Female WT adipocytes showed high Atgl expression, consistent with an adaptive capacity to mobilize stored triglycerides and limit excessive lipid accumulation [36]. This response was markedly reduced in female KO adipocytes, whereas male KO adipocytes showed increased Atgl expression, possibly reflecting compensatory lipid mobilization. This sex-specific difference suggests that female adipocytes may depend more strongly on Sirt3 to maintain lipolytic capacity, contributing to the pronounced lipid storage phenotype observed in female KO cells.

Based on evidence for enhanced lipogenic signaling and impaired lipid mobilization in female KO adipocytes, we next challenged female cells with bortezomib (BTZ), a proteasome inhibitor reported to activate AMPK and suppress lipogenic gene expression [24, 37]. In WT adipocytes, BTZ increased the pAMPK/AMPK ratio together with pAcc1/Acc1, consistent with activation of AMPK-dependent inhibitory phosphorylation of Acc1. In contrast, KO adipocytes showed low basal pAMPK/AMPK and failed to mount a comparable AMPK response to BTZ. Moreover, pAcc1/Acc1 remained reduced and Fasn levels remained elevated in KO cells, indicating persistence of a lipogenic state despite BTZ treatment. These data suggest that Sirt3 deficiency compromises the AMPK–Acc1 antilipogenic response in female adipocytes.

These signalling differences were accompanied by increased lipid storage. Oil Red O quantification and lipid droplet morphometry showed that KO adipocytes accumulated more lipids under basal conditions, and BTZ further enhanced this phenotype. Whereas WT adipocytes showed only modest lipid accumulation after BTZ treatment, KO cells displayed the highest Oil Red O signal together with increased droplet number and diameter. Qualitative light and transmission electron microscopy analyses complemented the quantitative lipid phenotype by revealing characteristic morphological and ultrastructural features. Semithin sections illustrated lipid-containing adipocyte-like cells, while TEM demonstrated lipid bodies, autophagic structures, and BTZ-associated ultrastructural alterations, with the most pronounced organelle changes observed in KO adipocytes. Although enlarged and rounded mitochondria and altered ER–mitochondria organization were observed in KO cells, these qualitative TEM images do not allow conclusions about mitochondrial mass or mitochondrial biogenesis. This distinction is relevant because recent proteomic analysis of human adipogenesis showed extensive cellular remodeling and spatial reorganization of metabolic pathways during adipocyte formation [38]. In addition, ATAD3

588 has recently been identified as a limiting factor for mitochondrial biogenesis, adipogenesis,
589 and lipogenesis in white adipocyte-like 3T3-L1 cells [39]. Although ATAD3 was not examined
590 in the present study, it represents a relevant future direction for testing whether Sirt3-
591 dependent mitochondrial regulation contributes to the sex-specific adipogenic phenotype
592 observed here. Therefore, the qualitative ultrastructural findings are consistent with, but do
593 not independently quantify, the increased lipid accumulation detected by Oil Red O staining
594 and lipid droplet morphometry. High magnification immunofluorescence imaging showed
595 that Acc1 signal was detectable in Oil Red O-positive adipocyte-like cells and appeared
596 enriched near lipid droplet associated regions, supporting qualitative localization of Acc1
597 within differentiated cells [40]. Together, these data support a model in which Sirt3 deficiency
598 impairs AMPK-dependent feedback inhibition of lipogenesis, while reduced Atgl limits
599 triglyceride mobilization, thereby favoring lipid accumulation in female KO adipocytes.
600 Building on the lipid droplet phenotype, fatty acid profiling and immunoblotting indicate that
601 Sirt3 loss is associated with the Scd1-linked desaturation phenotype. The C16:1/C16:0
602 desaturation index is widely used as a proxy for Scd1-dependent Δ9-desaturation [41]. In the
603 present study, this ratio was significantly higher in Sirt3 KO than WT adipocytes, indicating
604 increased palmitate-to-palmitoleate desaturation in the absence of Sirt3. This was
605 accompanied by markedly increased Scd1 protein abundance in KO adipocytes, particularly
606 under control conditions. Since Scd1-derived monounsaturated fatty acids can support
607 triglyceride synthesis and lipid droplet expansion [42], increased Scd1 abundance together
608 with an elevated C16:1/C16:0 ratio provides a plausible mechanism contributing to the lipid
609 storage phenotype of Sirt3-deficient adipocytes. Importantly, BTZ reduced Scd1 protein
610 abundance in KO cells but did not normalize the elevated C16:1/C16:0 ratio, suggesting that
611 the desaturation phenotype persists despite partial suppression of Scd1 protein levels. Thus,

Sirt3 deficiency appears to promote lipid deposition through coordinated changes in lipogenic signaling, lipid turnover, and Scd1-associated fatty acid desaturation [43]. In parallel, LC–MS metabolomics showed that BTZ primarily affected glycerophospholipid and lysophospholipid species in both WT and KO cells, indicating substantial membrane lipid remodeling [44]. In WT cells, enrichment of PE, PG, PS, LPC, and LPS species suggests broad glycerophospholipid turnover and may reflect stress-associated membrane remodeling, including pathways linked to phosphatidylserine dynamics during cellular stress [45]. In KO cells, PE, LPE, and PG species dominated the discriminant metabolites, further supporting membrane remodeling as a major BTZ-associated response. However, the metabolomic data did not reveal a clear genotype-specific signature explaining impaired AMPK-mediated adaptation under these experimental conditions. Taken together, these findings suggest that Sirt3 deficiency promotes lipid deposition through impaired AMPK–Acc1 antilipogenic signaling, reduced lipolytic capacity, and persistent Scd1-associated fatty acid desaturation, whereas BTZ induces phospholipid remodeling that is broadly conserved across genotypes.

Conclusion

The findings indicate that Sirt3 loss promotes a female-biased lipid storage phenotype associated with impaired AMPK–Acc1 antilipogenic signalling, increased *de novo* lipogenic markers, reduced lipolytic capacity, elevated Scd1 protein abundance, and a persistent increase in the C16:1/C16:0 desaturation index. Together, these results suggest that Sirt3 deficiency drives lipid accumulation through coordinated disruption of lipid synthesis, mobilization, and Scd1-associated fatty acid desaturation. A possible explanation for the stronger phenotype observed in female KO adipocytes is that female cells may rely more strongly on Sirt3-dependent mitochondrial and AMPK-linked metabolic control to maintain

635 the balance between lipid storage and lipid mobilization during adipogenic differentiation. In
636 this context, loss of Sirt3 may lower the capacity of female adipocytes to activate AMPK–Acc1-
637 dependent antilipogenic feedback, while simultaneously reducing lipolytic capacity and
638 promoting Scd1-associated fatty acid desaturation. Because this model uses male and female
639 MEF-derived adipocytes cultured under the same conditions, these differences may reflect,
640 at least in part, cell intrinsic sex dependent metabolic programming rather than acute
641 hormonal effects alone. Future studies should determine whether this female biased Sirt3-
642 dependent phenotype is conserved in primary adipocytes and adipose tissue in vivo. Further
643 work should also address whether sex hormones, sex chromosome complement, or
644 persistent epigenetic or metabolic programming contribute to the observed differences.
645 Mechanistically, it will be important to test whether restoration of AMPK–Acc1 signalling,
646 modulation of Scd1 activity, or enhancement of lipid turnover can reduce lipid accumulation
647 specifically in female Sirt3 deficient adipocytes.

648 Collectively, our results identify Sirt3 as a sex dependent regulator of adipocyte lipid
649 metabolism and support a model in which female adipocytes are particularly dependent on
650 Sirt3 to coordinate AMPK–Acc1 antilipogenic signalling, lipid turnover, and Scd1-associated
651 fatty acid desaturation during adipogenic differentiation. This provides a basis for future
652 studies addressing the mechanisms underlying female specific vulnerability to adipose lipid
653 dysregulation.

Declarations

Ethics approval

All animal-related procedures were approved by the Ministry of Agriculture of the Republic of Croatia and by the Ethics Committee of the Ruđer Bošković Institute, Zagreb, Croatia, under approval number HR-POK-003. The study was carried out in accordance with the guidelines and regulations of the Ministry of Agriculture of the Republic of Croatia and the Ethics Committee of the Ruđer Bošković Institute.

Consent for publication

Not applicable

Availability of data and materials

Data are available from the corresponding author upon request.

Competing interests

The authors declare no competing financial interests or personal relationships that could have influenced the work reported in this manuscript.

Funding

This work was funded by the Croatian Science Foundation, HrZZ IP-2022-10-4806.

Authors' contributions

Ena Šimunić: methodology, investigation, validation, writing - review & editing. **Kate Šešelja:** methodology, investigation, validation, writing – review & editing. **Iva I. Podgorski:** investigation, writing – review & editing. **Robert Belužić:** investigation, writing – review & editing. **Marijana Popović Hadžija**: methodology, investigation, writing – review & editing. **Marija Pinterić Mavar:** methodology, investigation, writing – review & editing. **Mirta Rešetar**: methodology, investigation, data curation, review & editing. **Mirna Halasz:** methodology,

investigation. **Morana Jaganjac:** methodology, investigation, formal analysis, data curation. **Ivana Tartaro Bujak:** methodology, investigation, formal analysis. **Marta Protrka:** methodology, investigation. **Tihomir Balog:** methodology, resources, writing – review & editing. **Sara Stojanović:** methodology, writing – review & editing. **Aleksandra Korać:** methodology, investigation, data curation, writing – review & editing. **Sandra Sobočanec:** conceptualization, supervision, writing – original draft, writing – review & editing, resources, formal analysis, funding acquisition.

Acknowledgements

The authors would like to thank Iva Pešun Međimorec for her excellent technical assistance and to Nina Junaković for her assistance in methodology. The authors would like to thank dr. sc. Vjekoslav Tomaić for generously providing bortezomib used in this study.

References

1. Costa DN, Santosa S, Jensen MD (2025) Sex differences in the metabolism of glucose and fatty acids by adipose tissue and skeletal muscle in humans. Physiol Rev 105:897–934

2. Chianelli M, Armellini M, Carpentieri M, et al (2025) Obesity in Prediabetic Patients: Management of Metabolic Complications and Strategies for Prevention of Overt Diabetes. Endocr Metab Immune Disord Drug Targets 25:8–36

3. Boulet N, Briot A, Galitzky J, Bouloumié A (2022) The Sexual Dimorphism of Human Adipose Depots. Biomedicines 10:2615

4. Torres Irizarry VC, Jiang Y, He Y, Xu P (2022) Hypothalamic Estrogen Signaling and

699 Adipose Tissue Metabolism in Energy Homeostasis. Front Endocrinol (Lausanne)
700 13:898139

701 5. Jo J, Gavrilova O, Pack S, Jou W, Mullen S, Sumner AE, Cushman SW, Periwal V (2009)
702 Hypertrophy and/or Hyperplasia: Dynamics of Adipose Tissue Growth. PLoS Comput
703 Biol 5:e1000324

704 6. Guo G, Wang W, Tu M, et al (2024) Deciphering adipose development: Function,
705 differentiation and regulation. Dev Dyn an Off Publ Am Assoc Anat 253:956–997

706 7. Dastagir K, Reimers K, Lazaridis A, et al (2014) Murine embryonic fibroblast cell lines
707 differentiate into three mesenchymal lineages to different extents: new models to
708 investigate differentiation processes. Cell Reprogram 16:241–252

709 8. Al-Sayegh MA, Mahmood SR, Abul Khair SB, Xie X, El Gindi M, Kim T, Almansoori A,
710 Percipalle P (2020) β-actin contributes to open chromatin for activation of the
711 adipogenic pioneer factor CEBPA during transcriptional reprograming. Mol Biol Cell
712 31:2511–2521

713 9. Al-Sayegh M, Ali H, Jamal MH, ElGindi M, Chanyong T, Al-Awadi K, Abu-Farha M (2021)
714 Mouse Embryonic Fibroblast Adipogenic Potential: A Comprehensive Transcriptome
715 Analysis. Adipocyte 10:1–20

716 10. Lee H, Yoon H (2024) Mitochondrial sirtuins: Energy dynamics and cancer metabolism.
717 Mol Cells 47:100029

718 11. Zhou Y, Chung ACK, Fan R, Lee HM, Xu G, Tomlinson B, Chan JCN, Kong APS (2017) Sirt3
719 Deficiency Increased the Vulnerability of Pancreatic Beta Cells to Oxidative Stress-
720 Induced Dysfunction. Antioxid Redox Signal 27:962–976

12. Lin Y, Yu K, Guo J (2025) Targeting SIRT3 to Ameliorate Diabetic Cardiomyopathy: Progress in Mechanistic Research and Prospects for Clinical Translation. J Diabetes 17:e70167

13. Hirschey MD, Shimazu T, Jing E, et al (2011) SIRT3 deficiency and mitochondrial protein hyperacetylation accelerate the development of the metabolic syndrome. Mol Cell 44:177–190

14. Pinterić M, Podgorski II, Hadžija MP, Bujak IT, Dekanić A, Bagarić R, Farkaš V, Sobočanec S, Balog T (2020) Role of sirt3 in differential sex-related responses to a high-fat diet in mice. Antioxidants 9:1–19

15. Pinterić M, Podgorski II, Popović Hadžija M, Tartaro Bujak I, Tadijan A, Balog T, Sobočanec S (2021) Chronic high fat diet intake impairs hepatic metabolic parameters in ovariectomized sirt3 ko mice. Int J Mol Sci. https://doi.org/10.3390/ijms22084277

16. Šimunić E, Podgorski II, Pinterić M, et al (2024) Sirtuin 3 drives sex-specific responses to age-related changes in mouse embryonic fibroblasts. Mech Ageing Dev. https://doi.org/10.1016/j.mad.2024.111996

17. Durkin ME, Qian X, Popescu NC, Lowy DR (2013) Isolation of Mouse Embryo Fibroblasts. Bio-protocol. https://doi.org/10.21769/bioprotoc.908

18. FOLCH J, LEES M, SLOANE STANLEY GH (1957) A simple method for the isolation and purification of total lipides from animal tissues. J Biol Chem 226:497–509

19. Perkovic MN, Jaganjac M, Milkovic L, et al (2023) Relationship between 4-Hydroxynonenal (4-HNE) as Systemic Biomarker of Lipid Peroxidation and Metabolomic Profiling of Patients with Prostate Cancer. Biomolecules.

https://doi.org/10.3390/biom13010145

20. Gil de la Fuente A, Godzien J, Fernández López M, Rupérez FJ, Barbas C, Otero A (2018) Knowledge-based metabolite annotation tool: CEU Mass Mediator. J Pharm Biomed Anal 154:138–149

21. Pang Z, Lu Y, Zhou G, et al (2024) MetaboAnalyst 6.0: towards a unified platform for metabolomics data processing, analysis and interpretation. Nucleic Acids Res 52:W398–W406

22. Lally JS V, Ghoshal S, DePeralta DK, et al (2019) Inhibition of Acetyl-CoA Carboxylase by Phosphorylation or the Inhibitor ND-654 Suppresses Lipogenesis and Hepatocellular Carcinoma. Cell Metab 29:174-182.e5

23. Xin T, Lu C (2020) SirT3 activates AMPK-related mitochondrial biogenesis and ameliorates sepsis-induced myocardial injury. Aging (Albany NY) 12:16224–16237

24. Oliva J, French SW, Li J, Bardag-Gorce F (2012) Proteasome inhibitor treatment reduced fatty acid, triacylglycerol and cholesterol synthesis. Exp Mol Pathol 93:26–34

25. Deshmukh RR, Dou QP (2015) Proteasome inhibitors induce AMPK activation via CaMKKβ in human breast cancer cells. Breast Cancer Res Treat 153:79–88

26. Attie AD, Krauss RM, Gray-Keller MP, et al (2002) Relationship between stearoyl-CoA desaturase activity and plasma triglycerides in human and mouse hypertriglyceridemia. J Lipid Res 43:1899–1907

27. Collins JM, Neville MJ, Pinnick KE, Hodson L, Ruyter B, van Dijk TH, Reijngoud D-J, Fielding MD, Frayn KN (2011) De novo lipogenesis in the differentiating human adipocyte can provide all fatty acids necessary for maturation. J Lipid Res 52:1683–

765 1692

766 28. Munir H, Ward LSC, Sheriff L, Kemble S, Nayar S, Barone F, Nash GB, McGettrick HM
767 (2017) Adipogenic Differentiation of Mesenchymal Stem Cells Alters Their
768 Immunomodulatory Properties in a Tissue-Specific Manner. Stem Cells 35:1636–1646

769 29. Alzaabi M, Khalili M, Sultana M, Al-Sayegh M (2024) Transcriptional Dynamics and Key
770 Regulators of Adipogenesis in Mouse Embryonic Stem Cells: Insights from Robust Rank
771 Aggregation Analysis. Int J Mol Sci. https://doi.org/10.3390/ijms25179154

772 30. Chen T, Liu J, Li N, Wang S, Liu H, Li J, Zhang Y, Bu P (2015) Mouse SIRT3 attenuates
773 hypertrophy-related lipid accumulation in the heart through the deacetylation of LCAD.
774 PLoS One 10:e0118909–e0118909

775 31. Barroso E, Rodríguez-Rodríguez R, Zarei M, Pizarro-Degado J, Planavila A, Palomer X,
776 Villarroya F, Vázquez-Carrera M (2020) SIRT3 deficiency exacerbates fatty liver by
777 attenuating the HIF1α-LIPIN 1 pathway and increasing CD36 through Nrf2. Cell
778 Commun Signal 18:1–13

779 32. Li Q, Spalding KL (2022) The regulation of adipocyte growth in white adipose tissue.
780 Front cell Dev Biol 10:1003219

781 33. Honecker J, Ruschke S, Seeliger C, et al (2022) Transcriptome and fatty-acid signatures
782 of adipocyte hypertrophy and its non-invasive MR-based characterization in human
783 adipose tissue. EBioMedicine 79:104020

784 34. Belužić R, Šimunić E, Podgorski II, Pinterić M, Hadžija MP, Balog T, Sobočanec S (2024)
785 Gene Expression Profiling Reveals Fundamental Sex-Specific Differences in SIRT3-
786 Mediated Redox and Metabolic Signaling in Mouse Embryonic Fibroblasts. Int J Mol Sci.

https://doi.org/10.3390/ijms25073868

35. Liu L-X, Zheng X-H, Hai J-H, Zhang C-M, Ti Y, Chen T-S, Bu P-L (2024) SIRT3 regulates cardiolipin biosynthesis in pressure overload-induced cardiac remodeling by PPARγ-mediated mechanism. PLoS One 19:e0301990

36. Zhang Z, Yu Z, Liang D, et al (2024) Roles of lipid droplets and related proteins in metabolic diseases. Lipids Health Dis 23:218

37. Min H, Xu M, Chen Z-R, Zhou J-D, Huang M, Zheng K, Zou X-P (2014) Bortezomib induces protective autophagy through AMP-activated protein kinase activation in cultured pancreatic and colorectal cancer cells. Cancer Chemother Pharmacol 74:167–176

38. Klingelhuber F, Frendo-Cumbo S, Omar-Hmeadi M, et al (2024) A spatiotemporal proteomic map of human adipogenesis. Nat Metab 6:861–879

39. Li S, Xu R, Yao Y, Rousseau D (2024) ATAD3 is a limiting factor in mitochondrial biogenesis and adipogenesis of white adipocyte-like 3T3-L1 cells. Cell Biol Int 48:1473–1489

40. Wijesinghe KM, Kim C-W, Schad EO, et al (2025) Plasma membrane accessible cholesterol is regulated by ACC1 and lipid droplets. bioRxiv Prepr Serv Biol. https://doi.org/10.1101/2025.08.21.671640

41. Lee JJ, Lambert JE, Hovhannisyan Y, Ramos-Roman MA, Trombold JR, Wagner DA, Parks EJ (2015) Palmitoleic acid is elevated in fatty liver disease and reflects hepatic lipogenesis. Am J Clin Nutr 101:34–43

42. Sun Q, Xing X, Wang H, Wan K, Fan R, Liu C, Wang Y, Wu W, Wang Y, Wang R (2024) SCD1 is the critical signaling hub to mediate metabolic diseases: Mechanism and the

development of its inhibitors. Biomed Pharmacother 170:115586

43. Hirschey MD, Shimazu T, Goetzman E, et al (2010) SIRT3 regulates mitochondrial fatty-acid oxidation by reversible enzyme deacetylation. 464:121–126

44. Ramalho MJ, Andrade S, Loureiro JA, Pereira MC (2022) Interaction of Bortezomib with Cell Membranes Regulates Its Toxicity and Resistance to Therapy. Membranes (Basel). https://doi.org/10.3390/membranes12090823

45. Furuta Y, Zhou Z (2023) How do necrotic cells expose phosphatidylserine to attract their predators-What's unique and what's in common with apoptotic cells. Front cell Dev Biol 11:1170551